Ionics (2024) 30:3605–3615
https://doi.org/10.1007/s11581-024-05544-y

RESEARCH

Electrostatic self-assembly of MoS_2/graphene hybrid films for energy storage in high-performance symmetric supercapacitor

Xiangxiang Du[1] · Shujun Liu[1] · Yanbiao Zhou[1] · Xuejun Shi[1] · Kesheng Cao[1]

Received: 8 March 2024 / Revised: 16 April 2024 / Accepted: 17 April 2024 / Published online: 22 April 2024

Abstract

A fabrication strategy involving the electrostatic self-assembly of positively charged molybdenum disulfide (MoS_2) nanosheets and negatively charged graphene oxide (GO) sheets and thermal reduction process is proposed to prepare MoS_2/graphene hybrid films. The incorporation of MoS_2 nanosheets embedded in graphene sheets serves as spacers, preventing the graphene sheets from restacking. The optimized free-standing MoS_2/graphene hybrid film (MoS_2/G-2) demonstrates a remarkable areal specific capacitance of 979 mF cm^{-2} at 1 mA cm^{-2}, which is 2.85 times as much as pure reduced graphene oxide (rGO) (343 mF cm^{-2}). Benefiting from the layer-layer self-assembly structure and good synergistic effect, MoS_2/G-2 electrode exhibits enhanced capacitive performance with excellent cycling stability and no capacitance attenuation after 3000 cycles. Furthermore, by utilizing MoS_2/G-2 as electrode material for the assembled symmetric supercapacitors (MoS_2/G-2// MoS_2/G-2), a superior areal energy density of 20 μWh cm^{-2} at the areal power density of 600 μW cm^{-2} is achieved. The prepared hybrid film materials hold immense potential in constructing high-performance film electrode for electrochemical energy storage.

Keywords Electrostatic self-assembly · Molybdenum disulfide · Graphene · Symmetric supercapacitors

Introduction

The development and design of high-performance energy storage devices have been motivated by the growing demand for sustainable and renewable energy sources. One promising alternative is supercapacitors (SCs) that possess a higher energy density compared to conventional capacitors and a superior power density than batteries [1–4]. They also have the advantages of a long life cycle, ultra-fast charge and discharge rates, and environmental friendliness [5, 6]. However, SCs typically have a limited energy density when compared to batteries, which usually constrains their practical applications. One efficient approach to increasing the energy density of SCs is enabling high cell voltage and/or specific capacitance. For aqueous or organic electrolyte systems, the voltage window is within a specific range. Therefore, adjusting the capacitance fully can result in an increase in energy density. The capacitive performance of SCs primarily relies on the electrode material, which involves two mechanisms for charge storage: electric double-layer capacitors (EDLC) by adsorption and accumulation of electrolyte ions, and pseudocapacitors by redox reactions at electrode/electrolyte interfaces [7, 8].

Two-dimensional (2D) graphene has been investigated for EDLC-type SC electrode material because of its exceptional physical and chemical properties. These properties include high specific surface area, mechanical strength, conductivity, and ultra-stable carbon structure [9–11]. However, graphene electrode materials tend to have relatively low capacitance because of the layer stacking and reduction of available surface area caused by van der Waals forces. In contrast, the graphene-like structure of MoS_2 has been identified as a promising SC electrode material. It possesses a unique S-Mo-S sandwich structure that affords a large surface area and exposed active edges [12–15]. MoS_2 offers excellent electrochemical performance as an active material, demonstrating high specific capacitance, charge storage capacity, and noticeable intrinsic ionic conductivity [16–18]. Inspired by these characteristics, combining MoS_2 and graphene to construct MoS_2/graphene hybrid has proven to be

✉ Xiangxiang Du
2791@pdsu.edu.cn

[1] School of Chemical and Environmental Engineering, Pingdingshan University, Pingdingshan 467000, People's Republic of China

an effective method to enhance the capacitive performance and energy density of graphene-based hybrids [19–25]. For instance, Maskhiwa et al. successfully prepared MoS_2/graphene foam composites through the hydrothermal process, resulting in a high-performance asymmetric supercapacitor cell. The composites exhibited a maximum specific capacitance of 59 F g^{-1} at 1 A g^{-1}, energy density of 16 Wh kg^{-1}, and power density of 758 W kg^{-1} [26]. Similarly, Yang et al. designed the MoS_2/GNS and MnO_2/GNS electrodes as the negative and positive electrodes for asymmetric supercapacitor, achieving a superior energy density of 78.9 Wh kg^{-1} at 284.1 W kg^{-1}. The prepared MoS_2/GNS negative electrode holds great potential in asymmetric supercapacitor owing to the wide voltage window and high specific capacitance [27]. Additionally, Saraf et al. synthesized MoS_2-rGO composite through the utilization of an optimized hydrothermal method and obtained a high specific capacitance of 387.6 F g^{-1} at 1.2 A g^{-1} [28]. The combination of MoS_2 and graphene has demonstrated superior electrochemical performance among various composites. Nevertheless, the traditional method of combining them without any interaction between the two components cannot effectively prevent the self-restacking of sheets and also affects electron motion and charge transfer at the interface [29, 30]. Therefore, it is imperative to explore the development of MoS_2/graphene electrode materials with interactive interfaces, ultimately leading to the attainment of enhanced electrochemical performance.

Herein, we present the fabrication process of MoS_2/graphene hybrid films through the electrostatic self-assembly. The nanosheets of MoS_2 with a positive charge were combined with GO with a negative charge through this technique, followed by a thermal reduction step. The resulting MoS_2/graphene hybrid films can act directly as working electrodes without any additives or binders. The MoS_2 nanosheets act as spacers and are embedded in the layers of graphene nanosheets to prevent the re-stacking of graphene and also increase its interlayer spacing. This provides an effective pathway for ion transport and ensures high-rate performance. The optimized hybrid film (MoS_2/G-2) exhibited a remarkable areal capacitance of 979 mF cm^{-2} at 1 mA cm^{-2}. Notably, this excellent capacitance remained unchanged even after 3000 charge/discharge cycles when subjected to a high current density of 10 mA cm^{-2}. To further evaluate the performance, symmetric supercapacitors (SSCs) were assembled with MoS_2/graphene hybrid film as electrode material. These SSCs exhibited a favourable areal energy density of 20 μWh cm^{-2} at the areal power density of 600 μW cm^{-2}, demonstrating excellent electrochemical energy storage characteristics.

Experimental

Materials

Sodium molybdate dihydrate (AR), poly(diallyldimethylammonium chloride) solution (PDDA, 35 wt%), thiourea (AR), concentrated sulfuric acid (98%), and acetone were obtained from Shanghai Macklin Biochemical Technology Co., Ltd. and employed without any additional purification.

Preparation of MoS_2 nanosheets

The MoS_2 nanosheets were prepared via a facile and optimized hydrothermal approach. Initially, 0.484 g of sodium molybdate dihydrate and 0.760 g of thiourea were dissolved in 30 mL of deionized water. After vigorous stirring for 10 min, the solution was transferred to a 50 mL autoclave and maintained at a temperature of 180 °C for 24 h. Subsequently, the reaction product was allowed to cool down to room temperature followed by filtration, thorough washing with deionized water, and ultimately subjected to freeze-drying for 3 h.

Preparation of MoS_2/graphene hybrid film (MoS_2/G)

The synthesis of GO was previously conducted via the modified Hummers method [31]. Forty milligrams of MoS_2 powder was exfoliated through ultrasonication in 20 mL of deionized water for 2 h. 0.5 mL of poly(diallyldimethylammonium chloride) solution (PDDA) was then added to the MoS_2 dispersion, followed by continuous stirring for 24 h. In a separate step, a dispersion of GO with a concentration of 2 mg/mL was prepared by dissolving 80 mg of GO in 40 mL of deionized water. This GO dispersion was then added into the above MoS_2/PDDA dispersion and stirred for 24 h at 25 °C. The MoS_2/GO film was formed using vacuum-assisted filtration with PVDF membrane (pore size, 0.22 μm). The MoS_2/GO film was further peeled off from the PVDF membrane dissolved in acetone. Finally, the hybrid MoS_2/GO film was kept at 350 °C for 5 h under nitrogen atmosphere to reduce GO and form the MoS_2/graphene hybrid film, denoted as MoS_2/G-2. By varying the mass ratio of MoS_2 and GO, other two different hybrid films were also prepared. Forty milligrams of MoS_2, 40 mg of GO (w:w = 1:1) and 80 mg of MoS_2, and 40 mg of graphene oxide (w:w = 2:1) according to the above similar operation steps to prepare the MoS_2/graphene hybrid films and denoted as MoS_2/G-1, MoS_2/G-3, respectively. As a control, only 80 mg of GO was used to form the film and recorded as rGO.

Characterization

The surface, cross-sectional morphology, and EDS element mapping of the samples were analyzed by scanning electron microscope (SEM, SU8010) equipped with an energy dispersive X-ray (EDX) detector. The chemical composition and structure of the samples were determined by X-ray diffraction patterns (XRD, Bruker D8 Advance, 2θ~10–80°, 5°/min), Raman spectroscopy (Raman shift ~50–2000 cm^{-1}, 633 nm laser excitation wavelength), and X-ray photoelectron spectroscopy (XPS, Thermo ESCALAB 250Xi, Al Kα).

Electrochemical measurements

To characterize the electrochemical performances of the MoS_2/graphene hybrid film (MoS_2/G), electrochemical measurements were conducted using an electrochemical workstation (CHI600E, Chenhua Instrument, Shanghai, China). In the three-electrode configuration, the hybrid film (0.8 × 0.8 cm^2) served as the working electrode, while the Pt plate functioned as a counter electrode. The reference electrode was Ag/AgCl and the electrolyte was 1 M H_2SO_4 solution. For the two-electrode system, two identical pieces of the MoS_2/graphene hybrid film were assembled into symmetric supercapacitors (SSCs) in 1 M H_2SO_4 electrolyte. Cyclic voltammetry (CV) measurements were performed in a potential window of 0–0.6 V with a scan rate of 10–100 mV/s. Galvanostatic charge/discharge (GCD) tests were conducted with a current density of 1–10 mA cm^{-2} within the same potential window. Cycling stability was evaluated by conducting 3000 repeated GCD test cycles at 10 mA cm^{-2}. Electrochemical impedance spectroscopy (EIS) was performed in the frequency range from 100 kHz to 0.01 Hz with an amplitude of 5 mV. The areal specific capacitance(C, mF cm^{-2}), areal energy density (E, μWh cm^{-2}), and areal power density (P, μW cm^{-2}) were calculated according to the Eqs. (1)–(4) [32, 33]:

$$C_{3-\text{electrode}} = \frac{I\Delta t}{A\Delta V} \tag{1}$$

$$C_{2-\text{electrode}} = \frac{2I\Delta t}{A\Delta V} \tag{2}$$

$$E = \frac{1}{2}C_{2-\text{electrode}}\Delta V^2\frac{1000}{3600} \tag{3}$$

$$P = \frac{E}{\Delta t}3600 \tag{4}$$

where $C_{3\text{-electrode}}$ and $C_{2\text{-electrode}}$ (mF cm^{-2}) represent the areal specific capacitance of electrodes in three-electrode and two-electrode cells; I/A (mA cm^{-2}) refers to current density; Δt (s) and ΔV (V) represent the discharge time and voltage window.

Results and discussion

Fabrication and characterization of the MoS_2/graphene hybrid film

The fabrication process of the MoS_2/graphene hybrid film (MoS_2/G) via electrostatic self-assembly and thermal reduction combining MoS_2 and graphene component was schematically illustrated in Fig. 1. The self-standing hybrid film was formed via filtering a mixed solution of PDDA-modified MoS_2 and GO on the PVDF filter membrane. The final thermal reduction treatment removed oxygen-containing groups in GO. To confirm the surface charge after the modification of MoS_2 by PDDA, PDDA-modified MoS_2 was positively charged with the zeta potential of +43.5 mV. Due to the abundant presence of oxygen-containing groups, GO acquired negative charge with the zeta potential of −35.9 mV. When positively charged MoS_2 was mixed with negatively charged GO, the mixture became viscous and the surface potential was altered to +23.1 mV, suggesting

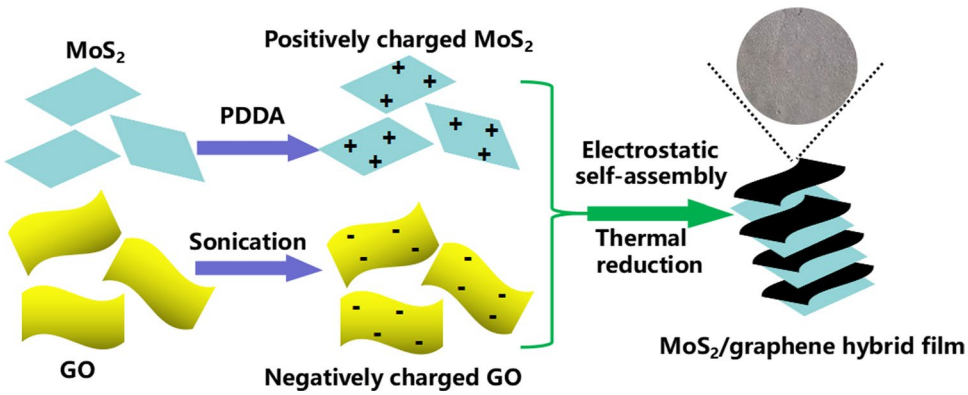

Fig. 1 Schematic fabrication route of MoS_2/graphene hybrid film (MoS_2/G)

successful electrostatic self-assembly between MoS_2 and GO.

The surface and interlayered structure morphology of the as-prepared samples were investigated by SEM. As displayed in Fig. 2a and b, it can be observed that the pure MoS_2 formed agglomerates and exhibited nanosheets ranging in size from 50 to 500 nm. The top-view SEM images of the MoS_2/graphene hybrid film in Fig. 2c revealed the distribution of graphene sheets and MoS_2 nanosheets on the surface. The cross-sectional SEM images of the MoS_2/graphene hybrid film in Fig. 2d and e depicted a hierarchical typical stacked layered structure with sufficient interlayer space for ion transport and volume change, which is suitable for rapid charging and discharging process [34]. The element mapping distribution of cross-sectional the MoS_2/graphene hybrid film can be further confirmed by the layer-layer self-assembly structure. The EDS mapping of C, O, S, and Mo elements was shown in Fig. 2f–i. All the elements were uniformly distributed on the cross-sectional surface of the sheets, suggesting the formation of layer-layer self-assembly structure.

Figure 3a shows the crystalline phase structures of pure MoS_2, rGO, and MoS_2/graphene hybrid film (MoS_2/G-2) by XRD. For pure MoS_2, the typical diffraction peaks at 13.2°, 32.9°, and 58.4° are ascribed to the crystal planes of (002), (100), and (110), respectively. These typical diffraction peaks match well with the hexagonal structure of MoS_2 (JCPDS: 37-1492) [27, 35]. The rGO film exhibits a broad peak at 24.7° attributed to the (002) plane, resulting from the stacking structure of the rGO sheets. Compared with rGO film, the (002) diffraction peak of MoS_2/G-2 is shifted towards a lower diffraction angle, suggesting an expansion of the interlayer distance. Additionally, MoS_2/G-2 shows three similar diffraction peaks to MoS_2, implying the insertion of MoS_2 nanosheets into the graphene sheets. Figure 3b shows Raman spectroscopy of MoS_2, rGO, and MoS_2/G-2. Obviously, two characteristic peaks are observed at approximately 377 cm^{-1} and 404 cm^{-1}, corresponding to two typical modes of in-plane vibration (E'_{2g}) and out-of-plane vibration (A_{1g}) of MoS_2 [36–38]. The hybrid film MoS_2/G-2 also exhibits the characteristic bands at 1343 cm^{-1} (D band) and 1592 cm^{-1} (G band) of rGO, as well as the peak at 388 cm^{-1} of MoS_2. The shift of the latter peak indicates an interaction between MoS_2 and graphene.

The chemical composition and bonding characteristics of the MoS_2/graphene hybrid film were determined by XPS.

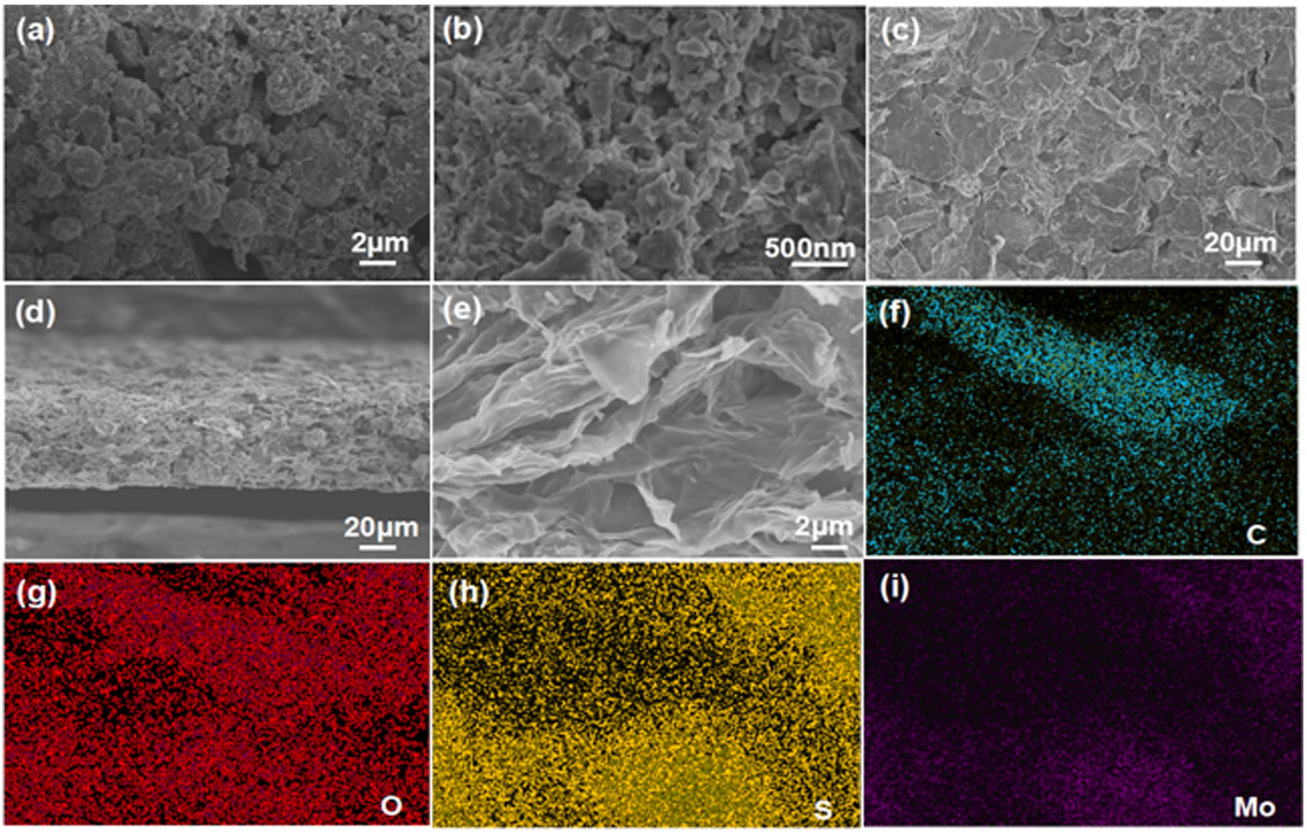

Fig. 2 SEM images of MoS_2 (**a**, **b**), MoS_2/graphene hybrid film (**c**), cross-sectional SEM images of MoS_2/graphene hybrid film (**d**, **e**), and cross-sectional EDS mapping of MoS_2/graphene hybrid film (**f**–**i**)

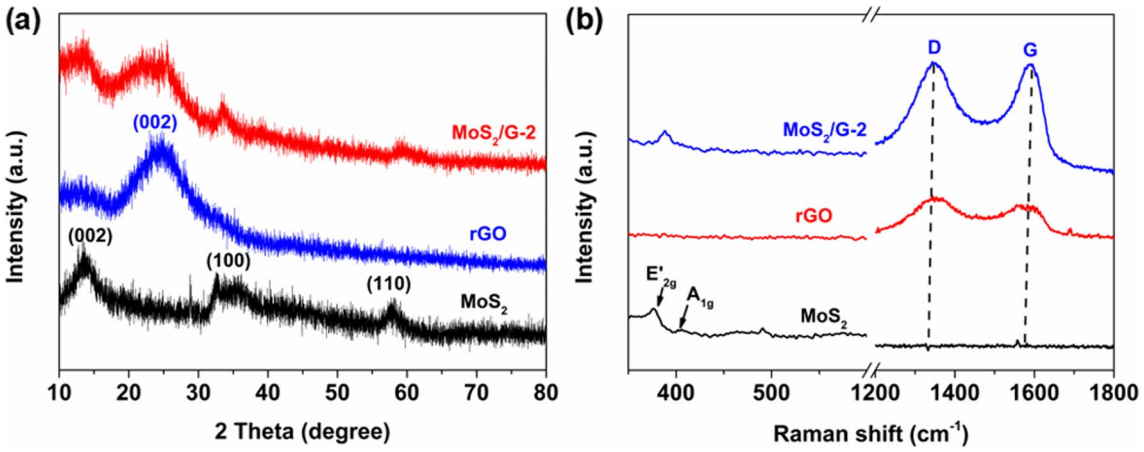

Fig. 3 XRD (**a**) and Raman spectra (**b**) of MoS_2, rGO, and MoS_2/G-2

Figure 4a shows the survey spectrum of MoS_2/G-2. The existence of surface elements C, O, Mo, and S indicates the successful synthesis of the MoS_2/graphene hybrid. The element contents of C 1s, O 1s, Mo 3d, and S 2p are 76.22 at%, 20.18 at%, 1.61 at%, and 1.98 at%, respectively. In Fig. 4b–d, the high-resolution spectra show more details. The C 1s spectrum is mainly composed of C-O (285.4 eV) and C-C (283.7 eV). The Mo 3d spectrum exhibits the Mo $3d_{3/2}$ (231.5 eV) and Mo $3d_{5/2}$ (230.3 eV) valence states, indicating that Mo^{+4} exists in MoS_2 [13, 39]. The peak at 234.7 eV can be considered Mo^{6+}, which may be attributed to the surface oxidation of MoS_2 to MoO_3 during the thermal

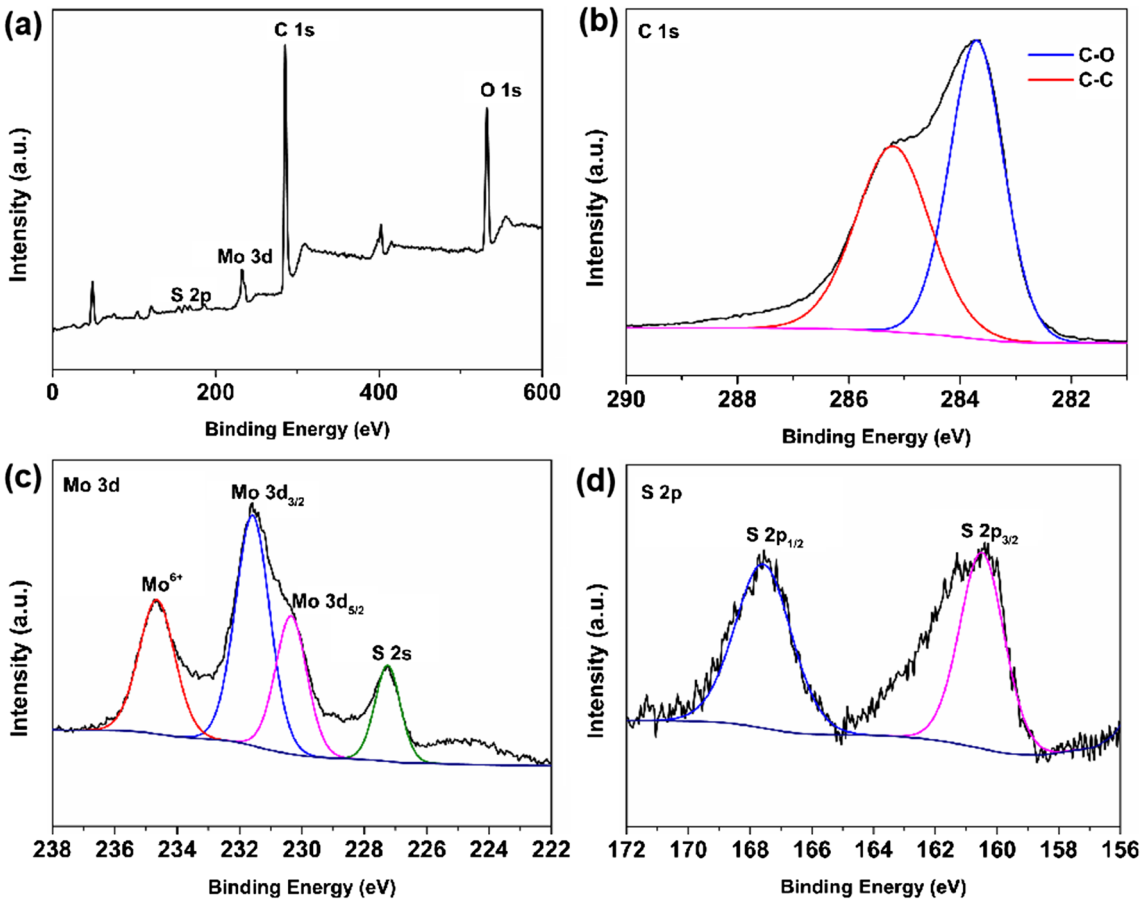

Fig. 4 XPS survey spectrum of MoS_2/G-2 (**a**) and high-resolution spectra of C 1s, Mo 3d, and S 2p (**b**–**d**)

reduction process. Furthermore, a typical peak at 227.2 eV is attributed to S 2s, confirming the presence of the S-Mo bond. In addition, the S 2p spectrum shows a doublet with the S $2p_{1/2}$ peak centered at 167.5 eV and the S $2p_{3/2}$ peak at 160.5 eV, which are in accordance with the divalent sulphide ions (S^{-2}) derived from MoS_2. These confirm the successful formation of the MoS_2/graphene hybrid frameworks.

Electrochemical performances of the MoS_2/graphene hybrid film

The as-prepared MoS_2/graphene hybrid films can directly act as working electrodes without any additives or binders and are expected to possess greatly enhanced electrochemical performances. CV was firstly conducted using a three-electrode system to investigate the electrochemical performances in 1 M H_2SO_4 acidic electrolyte. Figure 5a depicts the CV curves of the MoS_2/G-2 electrode, wherein various scan rates (10, 20, 30, 50, 80, 100 mV/s) were employed within a potential window of 0–0.6 V. These reversible closed CV curves exhibit relatively rectangular shapes without distinct redox peaks, indicating excellent capacitive behavior of the electrode. The CV curves still keep similar shapes even at 100 mV/s and the current increases with the increase of the scan rate, to some extent reflecting relatively the good rate capability [40, 41]. It is known that the integral area enclosed by the CV curve corresponds to the specific capacitance of the electrode material. Figure 5b compares the CV curves of MoS_2/G-1, MoS_2/G-2, MoS_2/G-3, and rGO electrodes at the same scan rate of 10 mV/s. As can be observed, the MoS_2/G-2 electrode demonstrates a larger integral area and higher specific capacitance relative to pure rGO and the other hybrid electrodes.

GCD measurements were conducted to further analyze the electrochemical performances of the as-fabricated electrode. The GCD curves of MoS_2/G-1, MoS_2/G-2, MoS_2/G-3, and rGO electrodes were performed at various current densities (1–10 mA cm^{-2}) within a potential window of 0–0.6 V (Fig. 6a–d). The GCD curves of rGO were found to be highly symmetrical and linear associated with the characteristic of electric double-layer capacitors. In contrast, the GCD curves of the three hybrid electrodes (MoS_2/G-1, MoS_2/G-2, MoS_2/G-3) displayed non-linear triangular charge/discharge patterns, indicating the presence of pseudocapacitance after the introduction of MoS_2. Notably, the discharge time of the MoS_2/G-2 electrode was significantly longer than those of pure rGO and the other two hybrid electrodes. This indicates the MoS_2/G-2 electrode possesses a higher specific capacitance consistent with the above CV results mentioned.

The areal specific capacitances of MoS_2/G-1, MoS_2/G-2, MoS_2/G-3, and rGO electrodes were calculated at various current densities from 1 to 10 mA cm^{-2} using the discharge curves shown in Fig. 7a. At different current densities of 1, 2, 3, 5, 8, and 10 mA cm^{-2}, the areal specific capacitances of MoS_2/G-2 were determined to be 979, 710, 602, 431, 243, and 164 mF cm^{-2}, respectively. Among all the MoS_2/graphene hybrid films and rGO, the MoS_2/G-2 electrode exhibited the highest areal specific capacitance. The maximum areal specific capacitance of MoS_2/G-2 was 2.85 times as much as pure rGO (343 mF cm^{-2}), showing an enhanced capacitive performance. Interestingly, it is observed that the areal specific capacitance of MoS_2/G-1 decreased compared to pure rGO, suggesting a lack of synergistic effect between MoS_2 and graphene. The addition of an appropriate amount of MoS_2 contributed to the improvement of the areal specific capacitance. The incorporation of MoS_2 nanosheets in the graphene layers acted as layer-structure spacers, preventing self-restacking and providing easy path for electrolyte ions to reach the inner layer of the electrode. This unique layer structure of electrostatic self-assembly effectively utilized the contribution of MoS_2 to Faraday capacitance and the strong synergistic effect of MoS_2 and graphene, and the improved conductivity

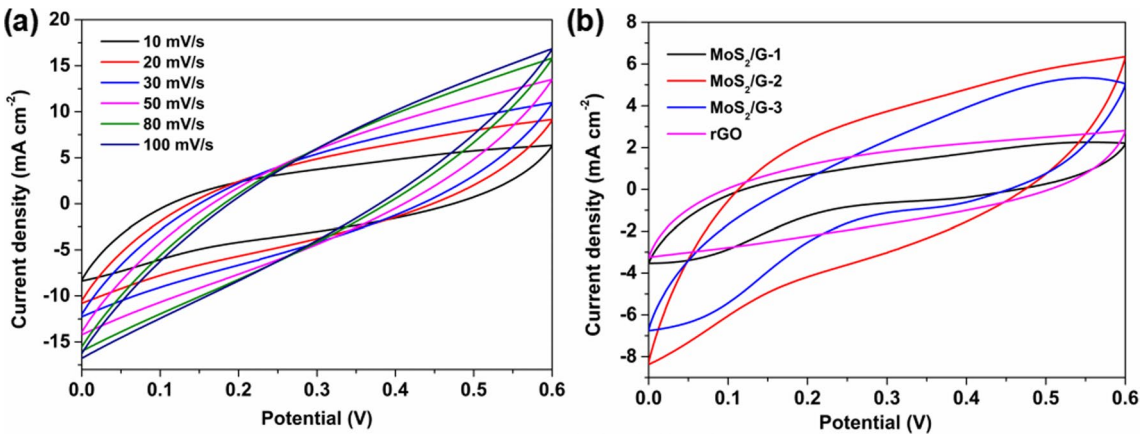

Fig. 5 CV curves of MoS_2/G-2 at 10–100 mV/s (**a**) and comparison of CV curves of MoS_2/G-1, MoS_2/G-2, MoS_2/G-3, and rGO at 10 mV/s (**b**)

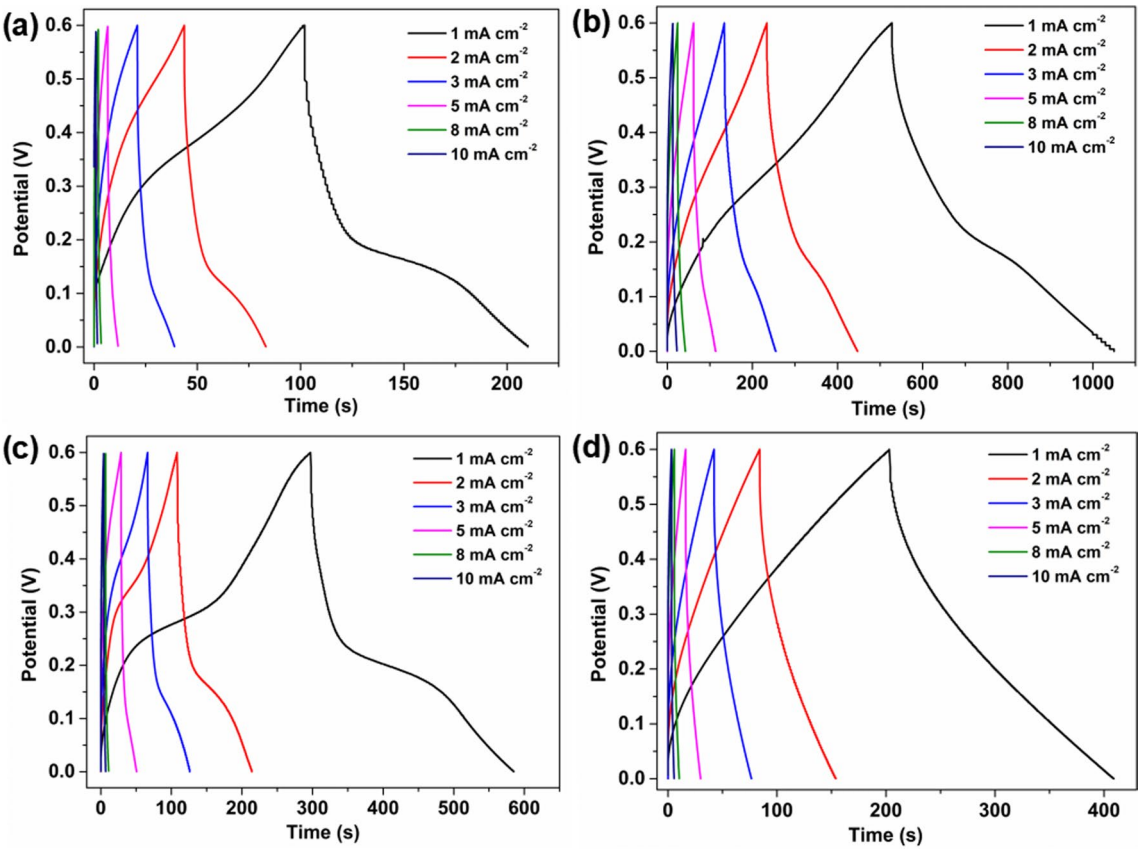

Fig. 6 GCD curves of MoS_2/G-1 (**a**), MoS_2/G-2 (**b**), MoS_2/G-3 (**c**), and rGO (**d**)

provided by graphene, resulting in the enhanced capacitive performance of MoS_2/G-2 electrode [42, 43]. Figure 7b presents the Nyquist plots of the fabricated electrodes. These plots mainly consisted of a linear part in the low-frequency region and a semicircular part in the high-frequency region. Among the hybrid film electrodes, the MoS_2/G-2 electrode possessed the smallest semicircle, demonstrating the lowest charge transfer resistance (Rct). At low frequencies, the MoS_2/G-2 electrode exhibited a steep linear slope similar to rGO, suggesting excellent capacitive behavior and superior ion transport. Additionally, the MoS_2/G-2 electrode had the smallest equivalent series resistance (Rs) value of 3.2 Ω compared to other electrodes. This can be attributed to the unique layer-layer self-assembly structure of MoS_2 and graphene, which prevents mutual self-stacking and reduces internal resistance.

Furthermore, Fig. 7c depicts the relationship between Z′ and $\omega^{-1/2}$ in the low-frequency region. The equation about the relationship between Z′ and $\omega^{-1/2}$ is $Z' = R + \sigma_w\omega^{-1/2}$. σ_w is the slope of the line Z′~$\omega^{-1/2}$. The corresponding fit slope values of MoS_2/G-1, MoS_2/G-2, MoS_2/G-3, and rGO electrodes are 44.66, 10.50, 22.35, and 13.45, respectively. It is observed that the MoS_2/G-2 electrode demonstrated the lowest slope in all electrodes, indicating the smallest ion diffusion resistance and the most efficient ion diffusion/transfer [44, 45]. This result further supports the enhanced areal specific capacitance of the MoS_2/graphene hybrid film. The cycling stability of MoS_2/G-2 electrode was depicted in Fig. 7d, with the GCD curves of the first and last several cycles shown in the inset. Notably, even after 3000 charge/discharge cycles at high current density, there was no capacitance decay, demonstrating an outstanding long-term electrochemical cycling life. The self-assembly layered structure of the hybrid electrode could provide stable backbone support, while the opened interlayer spacing allow for volume change, resulting in improved electrochemical cycling stability [46].

Electrochemical properties of the symmetric supercapacitors

The symmetric supercapacitors (SSCs) were assembled using free-standing MoS_2/G-2 films as symmetric electrodes in a two-electrode system to investigate their potential for practical applications. Figure 8a exhibits the CV curves of MoS_2/G-2-based SSCs at scan rates ranging from 10 to 100 mV/s. These CV curves exhibit similar shapes, consistent with the CV curves measured in three-electrode system. The

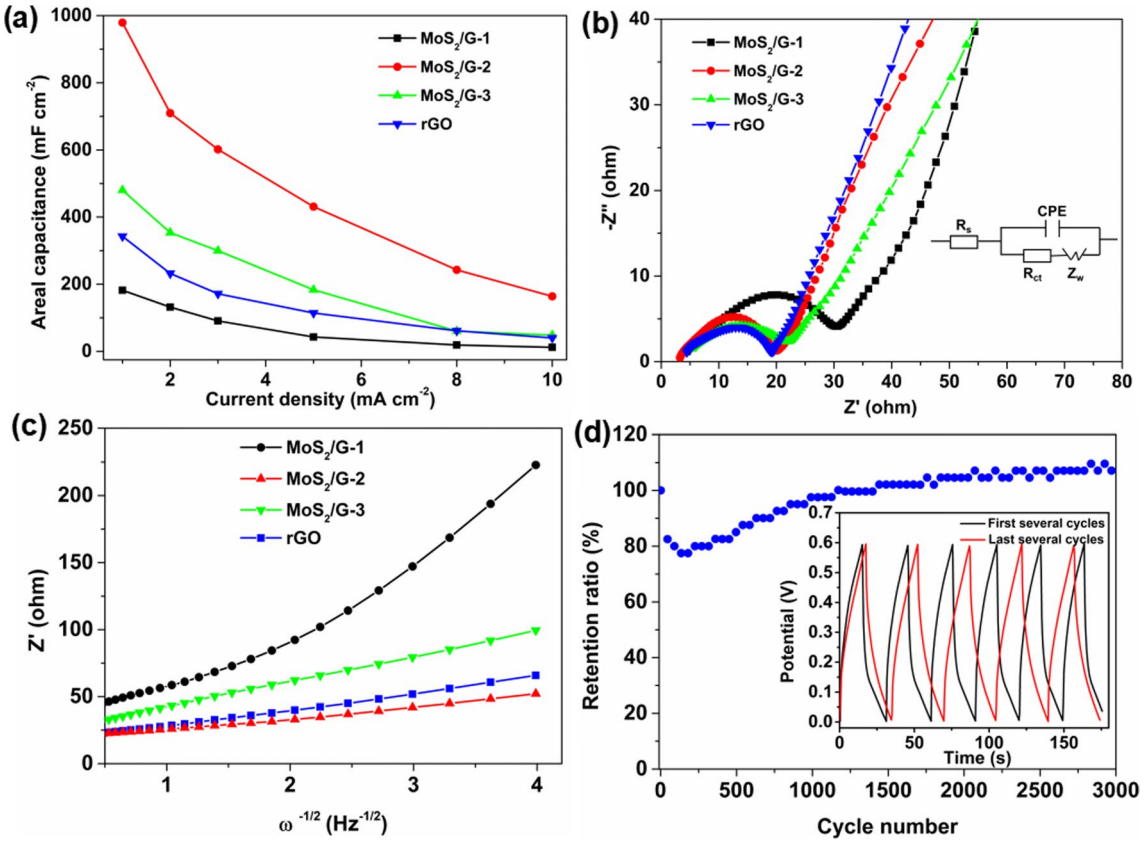

Fig. 7 Areal specific capacitance versus current density (**a**), Nyquist plots (**b**), and linear fitting the relationship between Z′ and $\omega^{-1/2}$ (**c**) of MoS_2/G-1, MoS_2/G-2, MoS_2/G-3, and rGO electrodes and cycling stability of MoS_2/G-2 electrode at 10 mA cm^{-2} (**d**)

GCD curves in Fig. 8b show approximately symmetric and linear profiles at all current densities, which indicates low charge transfer resistance within the electrode and efficient ion transport and diffusion. The areal specific capacitances of the assembled SSC device at different current densities were calculated according to the GCD curves and presented in Fig. 8c. It can be observed that the SSC device exhibited a maximum areal specific capacitance of 406 mF cm^{-2} at 1 mA cm^{-2}, and a minimum value of 97 mF cm^{-2} at 5 mA cm^{-2}. Energy density and power density are key performance indicators for evaluating the power supply performance of the fabricated SSC device. The Ragone plot in Fig. 8d illustrates the areal energy and power densities of the fabricated device. At a areal power density of 600 μW cm^{-2}, the SSCs achieved a maximum areal energy density of 20 μWh cm^{-2}. When the areal power density increased to 3000 μW cm^{-2}, the device still maintained an areal energy density of 5 μWh cm^{-2}. The fabricated MoS_2/G-2//MoS_2/G-2 device exhibited a superior areal energy density compared to previously reported MoS_2 and graphene-based devices, such as 1T/2H-MoS_2/GFT (8.61 μWh cm^{-2}) [47], graphene/MoS_2 (14.665 μWh cm^{-2}) [48], PEDOT:PSS/rGO/MoS_2 (8.5 μWh cm^{-2}) [49], MnO_2/RGO/CF (18.1 μWh cm^{-2}) [50], MoS_2/MnS/GR (7.0 μWh cm^{-2}) [32], and CNT/RGO (3.8 μWh cm^{-2}) [51].

Conclusions

The MoS_2/graphene hybrid films were designed and synthesized by combining negatively charged GO sheets with PDDA-modified positively charged MoS_2 nanosheets through electrostatic self-assembly and thermal reduction process. The optimum and binder-free hybrid film (MoS_2/G-2) electrode material exhibited remarkable areal capacitance of 979 mF cm^{-2} at 1 mA cm^{-2} and exceptional cycling stability with no capacitance decay after 3000 cycles. Compared to pure rGO and other hybrid films, the MoS_2/G-2 electrode showed an enhanced areal specific capacitance. This enhancement could be attributed to the efficient utilization of MoS_2 nanosheets and graphene, which possess a good synergistic effect and reduced electric resistance within layer-layer self-assembly structure, enabling rapid diffusion and transport of ions. Furthermore, for the potential practical application, the as-assembled symmetric supercapacitors (SSCs) based on MoS_2/graphene hybrid film demonstrated a maximum areal

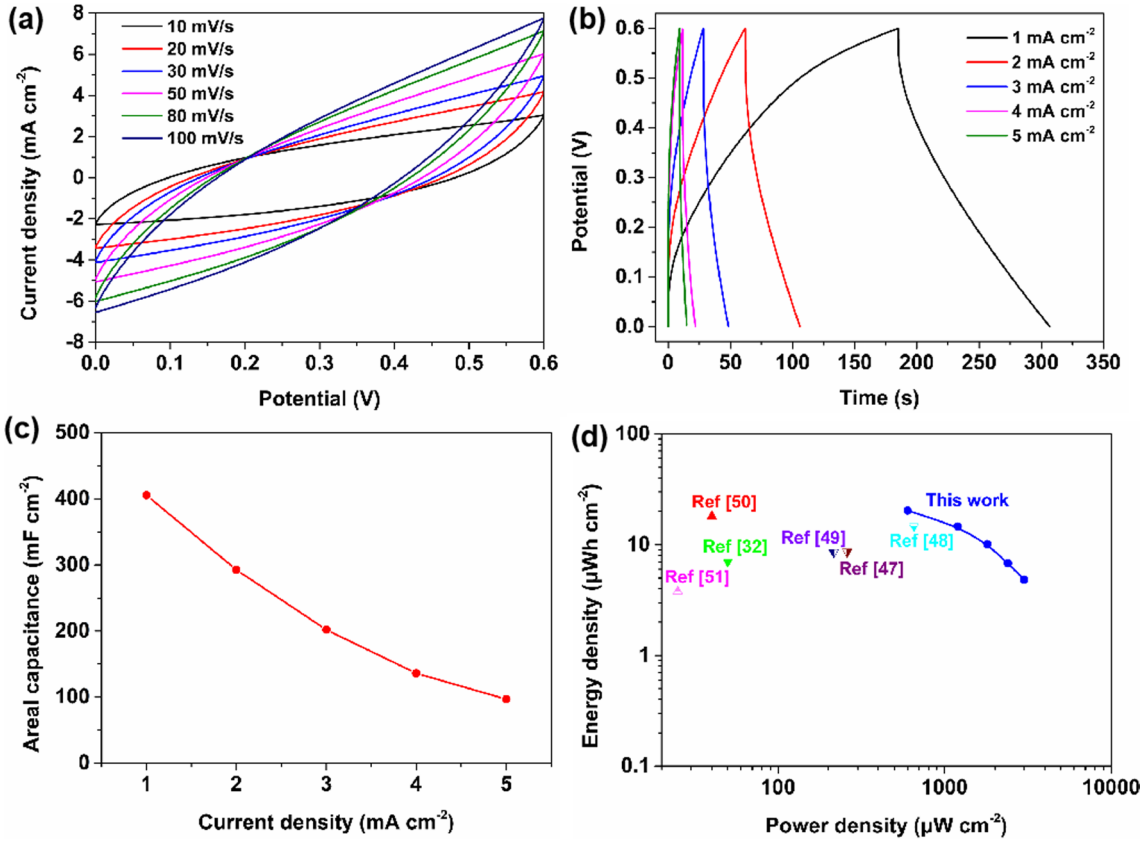

Fig. 8 CV curves (**a**), GCD curves (**b**), areal specific capacitance versus current density (**c**), and Ragone plot of the assembled symmetric supercapacitors device and other previously reported supercapacitors (**d**)

energy density of 20 μWh cm^{-2} at a areal power density of 600 μW cm^{-2}. These improvements in electrochemical performance and hybrid self-assembly structure suggest a potential for exploring high energy density supercapacitor devices.

Acknowledgements This work was supported by the Key Scientific Research Project in Colleges and Universities of Henan Province of China (No. 22B430024) and the Science and Technology Development Program of Henan province of China (No. 222102320057).

Data availability All data included in this study are available upon request by contact with the corresponding author.

Declarations

Competing interests The authors declare that they have no known competing financial interests or personal relationships that could have appeared to influence the work reported in this paper.

References

1. Qiu Z, Liu Z, Wang G, Huangfu C, Li Z, Yan Y, Chi C, Gao P, Lu X, Zhang S, Wei T, Fan Z (2023) Highly redox-active oligomers between graphene sheets as ultrahigh capacitance/rate and stable electrodes for supercapacitors. Energy Storage Mater 60:102824. https://doi.org/10.1016/j.ensm.2023.102824
2. El-Kady MF, Ihns M, Li M, Hwang JY, Mousavi MF, Chaney L, Lech AT, Kaner RB (2015) Engineering three-dimensional hybrid supercapacitors and microsupercapacitors for high-performance integrated energy storage. PNAS 112:4233–4238. https://doi.org/10.1073/pnas.1420398112
3. Zang X, Zhang R, Zhen Z, Lai W, Yang C, Kang F, Zhu H (2017) Flexible, temperature-tolerant supercapacitor based on hybrid carbon film electrodes. Nano Energy 40:224–232. https://doi.org/10.1016/j.nanoen.2017.08.026
4. Wang L, Han Y, Feng X, Zhou J, Qi P, Wang B (2016) Metal-organic frameworks for energy storage: batteries and supercapacitors. Coordin Chem Rev 307:361–381. https://doi.org/10.1016/j.ccr.2015.09.002
5. Inagaki M, Konno H, Tanaike O (2010) Carbon materials for electrochemical capacitors. J Power Sources 195:7880–7903. https://doi.org/10.1016/B978-0-12-407789-8.00011-9
6. Yu Z, Tetard L, Zhai L, Thomas J (2015) Supercapacitor electrode materials: nanostructures from 0 to 3 dimensions. Energy Environ Sci 8:702–730. https://doi.org/10.1039/c4ee03229
7. Muzaffar A, Ahamed MB, Deshmukh K, Thirumalai J (2019) A review on recent advances in hybrid supercapacitors: design, fabrication and applications. Renew Sust Energy Rev 101:123–145. https://doi.org/10.1016/j.rser.2018.10.026
8. Xu Y, Wang S, Peng H, Yang Z, Martin DJ, Bund A, Nanjundan AK, Yamauchi Y (2019) The interphase electrochemical characteristics of the cobaltosic oxide in organic electrolyte by Bode plots: double layer capacitance and pseudocapacitance. ChemElectroChem 6:2456–2463. https://doi.org/10.1002/celc.201900289

9. Han Y, Ge Y, Chao Y, Wang C, Wallace GG (2018) Recent progress in 2D materials for flexible supercapacitors. J Energy Chem 27:57–72. https://doi.org/10.1016/j.jechem.2017.10.033
10. Gandara M, Gonçalves ES (2020) Polyaniline supercapacitor electrode and carbon fiber graphene oxide: electroactive properties at the charging limit. Electrochim Acta 345:136197. https://doi.org/10.1016/j.electacta.2020.136197
11. Tian P, Zang J, Jia S, Zhang Y, Gao H, Zhou S, Wang W, Xu H, Wang Y (2018) Preparation of S/N co-doped graphene through a self-generated high gas pressure for high rate supercapacitor. Appl Surf Sci 456:781–788. https://doi.org/10.1016/j.apsusc.2018.06.213
12. Ye G, Gong Y, Lin J, Li B, He Y, Pantelides ST, Zhou W, Vajtai R, Ajayan PM (2016) Defects engineered monolayer MoS_2 for improved hydrogen evolution reaction. Nano Lett 16:1097–1103. https://doi.org/10.1021/acs.nanolett.5b04331
13. Liu MC, Xu Y, Hu YX, Yang QQ, Kong LB, Liu WW, Niu WJ, Chueh YL (2018) Electrostatically charged MoS_2/graphene oxide hybrid composites for excellent electrochemical energy storage devices. ACS Appl Mater Interfaces 10:35571–35579. https://doi.org/10.1021/acsami.8b09085
14. Zhang X, Zhang M, Tian Y, You J, Yang C, Su J, Li Y, Gao Y, Gu H (2018) In situ synthesis of MoS_2/graphene nanosheets as free-standing and flexible electrode paper for high-efficiency hydrogen evolution reaction. RSC Adv 8:10698–10705. https://doi.org/10.1039/C8RA01226A
15. Liang J, Wang C, Zhao P, Wang Y, Ma L, Zhu G, Hu Y, Lu Z, Xu Z, Ma Y, Chen T, Tie Z, Liu J, Jin Z (2018) Interface engineering of anchored ultrathin TiO_2/MoS_2 heterolayers for highly-efficient electrochemical hydrogen production. ACS Appl Mater Interfaces 10:36084–36089. https://doi.org/10.1021/acsami.7b19009
16. Bello IT, Oladipo AO, Adedokun O, Dhlamini SM (2020) Recent advances on the preparation and electrochemical analysis of MoS_2-based materials for supercapacitor applications: a mini-review. Mater Today Commun 25:101664. https://doi.org/10.1016/j.mtcomm.2020.101664
17. Gao YP, Huang KJ, Wu X, Hou ZQ, Liu YY (2018) MoS_2 nanosheets assembling three-dimensional nanospheres for enhanced-performance supercapacitor. J Alloys Compd 741:174–181. https://doi.org/10.1016/j.jallcom.2018.01.110
18. Sarkar D, Das D, Das S, Kumar A, Patil S, Nanda KK, Sarma DD, Shukla A (2019) Expanding interlayer spacing in MoS_2 for realizing an advanced supercapacitor. ACS Energy Lett 4:1602–1609. https://doi.org/10.1021/acsenergylett.9b00983
19. Huang KJ, Wang L, Liu YJ, Liu YM, Wang HB, Gan T, Wang LL (2013) Layered MoS_2-graphene composites for supercapacitor applications with enhanced capacitive performance. Int J Hydrogen Energy 38:14027–14034. https://doi.org/10.1016/j.ijhydene.2013.08.112
20. Da Silveira Firmiano EG, Rabelo AC, Dalmaschio CJ, Pinheiro AN, Pereira EC, Schreiner WH, Leite ER (2014) Supercapacitor electrodes obtained by directly bonding 2D MoS_2 on reduced graphene oxide. Adv Energy Mater 4:1–8. https://doi.org/10.1002/aenm.201301380
21. Bai LZ, Wang YH, Cheng SS, Li F, Zhang ZY, Liu YQ (2018) Synthesis and electrochemical performance of molybdenum disulfide-reduced graphene oxide-polyaniline ternary composites for supercapacitors. Front Chem 6:1–7. https://doi.org/10.3389/fchem.2018.00218
22. Thangappan R, Kalaiselvam S, Elayaperumal A, Jayavel R, Arivanandhan M, Karthikeyan R, Hayakawa Y (2016) Graphene decorated with MoS_2 nanosheets: a synergetic energy storage composite electrode for supercapacitor applications. Dalton Trans 45:2637–2646. https://doi.org/10.1039/C5DT04832J
23. Jhankal D, Khan MS, Jhankal KK, Sachdev K (2023) Charge storage kinetics of MoS_2 flower decorated reduced graphene oxide for quasi solid-state symmetric supercapacitor. J Phys Chem Solids 173:111117. https://doi.org/10.1016/j.jpcs.2022.111117
24. Bongu CS, Krishnan MR, Soliman A, Arsalan M, Alsharaeh EH (2023) Flexible and freestanding MoS2/graphene composite for high-performance supercapacitors. ACS Omega 8:36789–36800. https://doi.org/10.1021/acsomega.3c03370
25. Kumar P, Sharma S, Jabeen S, Samra KS (2022) Hybrid microwave annealing assisted synthesis of MoS_2-RGO nanostructures: optimization and characterization for application in supercapacitors. Electrochim Acta 426:140738. https://doi.org/10.1016/j.electacta.2022.140738
26. Patil UM, Nam MS, Kang S, Sohn JS, Sim HB, Kang S, Jun SC (2016) Fabrication of ultra-high energy and power asymmetric supercapacitors based on hybrid 2D MoS_2/graphene oxide composite electrodes: a binder-free approach. RSC Adv 6:43261–43271. https://doi.org/10.1039/C6RA00670A
27. Yang X, Niu H, Jiang H, Wang Q, Qu F (2016) High energy density all-solid-state asymmetric supercapacitor based on MoS_2/graphene nanosheet and MnO_2/graphene hybrid electrodes. J Mater Chem A 4:11264–11275. https://doi.org/10.1039/C6TA03474H
28. Saraf M, Natarajan K, Mobin SM (2018) An emerging robust heterostructure of MoS_2-rGO for high-performance supercapacitors. ACS Appl Mater Interfaces 10:16588–16595. https://doi.org/10.1021/acsami.8b04540
29. Joseph N, Muhammed Shafi P, Bose AC (2020) Recent advances in 2D-MoS_2 and its composite nanostructures for supercapacitor electrode application. Energy Fuels 34:6558–6597. https://doi.org/10.1021/acs.energyfuels.0c0043
30. Ansari SA, Fouad H, Ansari SG, Sk MP, Cho MH (2017) Mechanically exfoliated MoS_2 sheet coupled with conductive polyaniline as a superior supercapacitor electrode material. J Colloid Interface Sci 504:276–282. https://doi.org/10.1016/j.jcis.2017.05.064
31. Du X, Shi X, Li Y, Cao K (2020) Construction of N, S-co-doped graphene/polyaniline composite as free-standing electrode material. Int J Energy Res 45:6227–6238. https://doi.org/10.1002/er.6243
32. Zhou C, Hong M, Yang Y, Yang C, Hu N, Zhang L, Yang Z, Zhang Y (2019) Laser-induced bi-metal sulfide/graphene nanoribbon hybrid frameworks for high-performance all-in-one fiber supercapacitors. J Power Sources 438:227044. https://doi.org/10.1016/j.jpowsour.2019.227044
33. Chang Y, Shi H, Yan X, Zhang G, Chen L (2020) A ternary B, N, P-Doped carbon material with suppressed water splitting activity for high-energy aqueous supercapacitors. Carbon 170:127–136. https://doi.org/10.1016/j.carbon.2020.08.013
34. Zhou Y, Wang X, Acauan L, Kalfon-Cohen E, Ni X, Stein Y, Gleason KK, Wardle BL (2019) Ultrahigh-areal-capacitance flexible supercapacitor electrodes enabled by conformal P3MT on horizontally aligned carbon-nanotube arrays. Adv Mater 31:1901916. https://doi.org/10.1002/adma.201901916
35. Choi SH, Kang YC (2015) Polystyrene-templated aerosol synthesis of MoS_2-amorphous carbon composite with open macropores as battery electrode. ChemSusChem 8:2260–2267. https://doi.org/10.1002/cssc.201500063
36. David L, Bhandavat R, Singh G (2014) MoS_2/graphene composite paper for sodium-ion battery electrodes. ACS Nano 8:1759–1770. https://doi.org/10.1021/nn406156b
37. Gołasa K, Grzeszczyk M, Bożek R, Leszczyński P, Wysmołek A, Potemski M, Babiński A (2014) Resonant Raman scattering in MoS_2-from bulk to monolayer. Solid State Commun 197:53–56. https://doi.org/10.1016/j.ssc.2014.08.009
38. Cao Y (2021) Roadmap and direction towards high performance MoS_2 hydrogen evolution catalysts. ACS Nano 15:11014–11039. https://doi.org/10.1021/acsnano.1c01879
39. Wang N, Pan Q, Yang X, Zhu H, Ding G, Jia Z, Wu Y, Zhao L (2019) High performance asymmetric supercapacitor based on

Ni_xS_y/MoS_2 nanoparticles. ACS Appl Nano Mater 2:4910–4920. https://doi.org/10.1021/acsanm.9b00874
40. Zeng R, Li Z, Li L, Li Y, Huang J, Xiao Y, Yuan K, Chen Y (2019) Covalent connection of polyaniline with MoS_2 nanosheets toward ultrahigh rate capability supercapacitors. ACS Sustainable Chem Eng 7:11540–11549. https://doi.org/10.1021/acssuschemeng.9b01442
41. He C, Liang Y, Gao P, Long C, Shi D, Xie X, Li RK-Y, Yang Y (2017) Bioinspired Co_3O_4 /graphene layered composite films as self-supported electrodes for supercapacitors. Compos Part B 121:68–74. https://doi.org/10.1016/j.compositesb.2017.03.025
42. Masikhwa TM, Madito MJ, Bello A, Dangbegnon JK, Manyala N (2017) High performance asymmetric supercapacitor based on molybdenum disulphide/graphene foam and activated carbon from expanded graphite. J Colloid Interf Sci 488:155–165. https://doi.org/10.1016/j.jcis.2016.10.095
43. Zhuo Y, Prestat E, Kinloch IA, Bissett MA (2022) Self-assembled 1T-MoS_2/functionalized graphene composite electrodes for supercapacitor devices. ACS Appl Energy Mater 5:61–70. https://doi.org/10.1021/acsaem.1c02203
44. Yan J, Ren CE, Maleski K, Hatter CB, Anasori B, Urbankowski P, Sarycheva A, Gogotsi Y (2017) Flexible Mxene/graphene films for ultrafast supercapacitors with outstanding volumetric capacitance. Adv Funct Mater 27:1701264. https://doi.org/10.1002/adfm.201701264
45. Zheng F, Wei Z, Xia H, Tu Y, Meng X, Zhu K, Zhao J, Zhu Y, Zhang J, Yang Y, Deng D (2022) 3D MoS_2 foam integrated with carbon paper as binder-free anode for high performance sodium-ion batteries. J Energy Chem 65:26–33. https://doi.org/10.1016/j.jechem.2021.05.021
46. Sarmah D, Kumar A (2021) Symmetric supercapacitors with layer-by-layer Molybdenum disulfide-reduced graphene oxide structures and poly(3,4-ethylenedioxythiophene) nanoparticles nanohybrid electrode. J Energy Storage 35:102289. https://doi.org/10.1016/j.est.2021.102289
47. Zhang C, Ning J, Wang B, Guo H, Feng X, Shen X, Jia Y, Dong J, Wang D, Zhang J, Hao Y (2021) Hybridized 1T/2H-MoS_2/graphene fishnet tube for high-performance on-chip integrated micro-systems comprising supercapacitors and gas sensors. Nano Res 14:114–121. https://doi.org/10.1007/s12274-020-3052-x
48. Tang M, Wu Y, Yang J, Xue Y (2020) Hierarchical core-shell fibers of graphene fiber/radially-aligned molybdenum disulfide nanosheet arrays for highly efficient energy storage. J Alloys Compd 828:153622. https://doi.org/10.1016/j.jallcom.2019.153622
49. Zhou Q, Lv G, Wang X, Teng W, Hu P, Du Y, Li H, Hu Y, Liu W, Wang J (2023) Constructing a hierarchical ternary hybrid of PEDOT:PSS/rGO/MoS_2 as an efficient electrode for a flexible fiber-shaped supercapacitor. ACS Appl Energy Mater 6:5797–5805. https://doi.org/10.1021/acsaem.3c00187
50. Zhang Z, Xiao F, Wang S (2015) Hierarchically structured MnO_2/graphene/carbon fiber and porous graphene hydrogel wrapped copper wire for fiber-based flexible all-solid-state asymmetric supercapacitors. J Mater Chem A 3:11215–11223. https://doi.org/10.1039/c5ta02331a
51. Wang B, Fang X, Sun H, He S, Ren J, Zhang Y, Peng H (2015) Fabricating continuous supercapacitor fibers with high performances by integrating all building materials and steps into one process. Adv Mater 27:7854–7860. https://doi.org/10.1002/adma.201503441